

# AdaptIR: Parameter Efficient Multi-task Adaptation for Pre-trained Image Restoration Models

Hang Guo<sup>1</sup>, Tao Dai<sup>2,\*</sup>, Yuanchao Bai<sup>3</sup>, Bin Chen<sup>3</sup>, Shu-Tao Xia<sup>1,4</sup>, Zexuan Zhu<sup>2</sup>

<sup>1</sup>Tsinghua University, <sup>2</sup>Shenzhen University,

<sup>3</sup>Harbin Institute of Technology, <sup>4</sup>Peng Cheng Laboratory

{cshguo, daitao.edu, yuanchao.bai}@gmail.com, chenbin2021@hit.edu.cn,

xiast@sz.tsinghua.edu.cn, zhuzx@szu.edu.cn

## Abstract

Pre-training has shown promising results on various image restoration tasks, which is usually followed by full fine-tuning for each specific downstream task (e.g., image denoising). However, such full fine-tuning usually suffers from the problems of heavy computational cost in practice, due to the massive parameters of pre-trained restoration models, thus limiting its real-world applications. Recently, Parameter Efficient Transfer Learning (PETL) offers an efficient alternative solution to full fine-tuning, yet still faces great challenges for pre-trained image restoration models, due to the diversity of different degradations. To address these issues, we propose AdaptIR, a novel parameter efficient transfer learning method for adapting pre-trained restoration models. Specifically, the proposed method consists of a multi-branch inception structure to orthogonally capture local spatial, global spatial, and channel interactions. In this way, it allows powerful representations under a very low parameter budget. Extensive experiments demonstrate that the proposed method can achieve comparable or even better performance than full fine-tuning, while only using 0.6% parameters. Code is available at <https://github.com/csguoh/AdaptIR>.

## 1. Introduction

Image restoration, aiming to recover high-quality images from their degraded counterparts, is a fundamental and long-standing problem in computer vision and further has a wide range of sub-problems, including super-resolution, image denoising, deraining, low-light image enhancement, etc. Early researches [18, 54, 68] typically focus on studying each task independently, while neglecting the inherent relationships between different tasks. As a result, previous methods usually have limited generalization for different

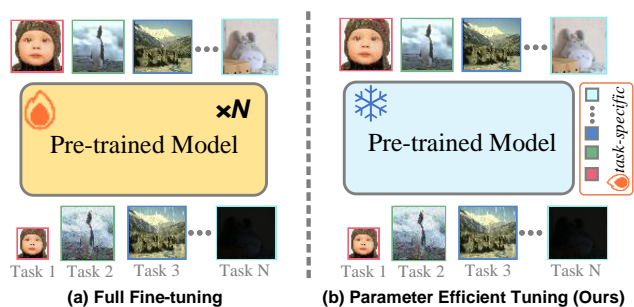


Figure 1. The previous full fine-tuning paradigm (a) assigns separate weights to each downstream task, leading to huge training and storage overheads. Our parameter-efficient tuning paradigm (b) only trains and saves a small number of parameters when continuously adding new unseen tasks.

image restoration tasks.

To improve the generalization ability, pre-training has recently been introduced to image restoration and gained promising results [8, 34]. It usually first pre-trains models on multiple image restoration tasks with vast synthetic datasets [15] to learn similarities between different tasks, followed by fine-tuning for specific downstream tasks. Although full fine-tuning offers an intuitive manner to adapt pre-trained models to downstream tasks, it raises great concerns regarding its training and storage efficiency because it requires training and saving a separate copy of parameters for each task (see Fig. 1(a)), which greatly limits real-world applications. Recently, Parameter Efficient Transfer Learning (PETL), as an alternative solution to full fine-tuning, requires training only a small part of task-specific parameters. Although PETL methods have been extensively studied on natural language [3, 22, 31] and high-level vision [10, 12, 41, 67], it has been less explored in low-level image restoration tasks.

Despite the success of PETL methods in high-level computer vision tasks, it still faces great challenges for low-level image restoration tasks. *First*, existing PETL methods can work well on specific degradation, while failing to general-

\*Corresponding author: Tao Dai

ize across multiple degradations. As shown in [49], different restoration tasks have different model preferences, *e.g.*, super-resolution prefers high-pass while denoising prefers low-pass. Therefore, the single-branch structure of existing PETL methods [9, 22, 29] limits them to be only specific-pass, thus preventing versatility under multiple degradations. *Second*, when faced with more challenging unseen tasks, such as second-order degradation [16, 59], current methods suffer from substantial performance degradation. This is because the current PETL approaches are designed for whole-image-level semantic understanding [9, 26, 63], and thus is limited when applied to low-level vision which needs to fully exploit the internal statistics such as neighborhood similarity and patch recurrence [48, 73]. For instance, some methods [9, 22, 36] only consider channel interactions without utilizing spatial dependencies, and this insufficient representation leads to sub-optimal restoration results. The aforementioned observations motivate us to develop a *versatile* and *powerful* adaptation strategy for pre-trained image restoration models.

To address the above challenges, we propose a novel PETL method, dubbed AdaptIR, for adapting pre-trained image restoration models to various downstream tasks (see Fig. 1(b)). In order to maintain generic performance under multiple degradations, we draw inspiration from the Mixture-of-Experts (MoE) [32, 55, 72] and propose a multi-branch inception structure, where each branch can be viewed as an expert specialized in restoration from a certain perspective. Moreover, to develop a strong representation for hard tasks under a low parameter budget, we introduce three modules, which perform in parallel branches with orthogonal spatial-channel modeling. Concretely, we introduce the Local Interaction Module (LIM) which employs depth-separable convolution [23] with kernel weight decomposition to exploit the local neighborhood similarity. We further consider modeling the global patch recurrence, and develop the Frequency Affine Module (FAM) which performs frequency depth-separable affine transformation to introduce global dependency while using few parameters. Finally, the Channel Shift Module (CSM) is used to model channel interactions, which can compensate for the information loss of previous depth-separable strategies.

The contributions of our work are as follows:

- We propose AdaptIR, an accustomed PETL method for low-level image restoration, to fully exploit the internal statistics in images. To the best of our knowledge, it is the first work to explore the parameter-efficient adaptation for pre-trained image restoration models.
- We propose three orthogonal modules placed in parallel branches to implement spatial-channel modelling, which allows for versatile and powerful adaptation under a low parameter budget.
- Extensive experiments on various downstream tasks in-

dicating the proposed AdaptIR outperforms other strong PETL baselines with favorable generalization ability.

## 2. Related Work

### 2.1. Pre-training in Image Restoration

Image restoration has attracted a lot of research interest in recent years. Due to the challenging ill-posed nature, some early research paradigms typically study each sub-task in image restoration independently and have recently achieved favorable progress in their respective fields [14, 62, 68, 69]. However, designing a specific model for each task is cumbersome, and does not consider the similarities among different tasks. Recently, motivated by the success of pre-training in natural language processing [6, 17, 51, 52] and other high-level vision tasks [4, 21, 61], some recent works [8, 34, 39, 40] have introduced this technique to image processing tasks. For example, IPT [8] first trains a multi-task shared ViT backbone using synthetic data from ImageNet [15] dataset and then fine-tunes on specific downstream datasets. EDT [34] proposes a multi-related-task pre-training technique and introduces window-attention for effective pre-training. Although these approaches have yielded promising results, however, they typically need to fully fine-tune the large pre-trained model for each specific task, which incurs significant training and storage costs.

### 2.2. Parameter-Efficient Transfer Learning

Parameter efficient transfer learning, which initially came from with NLP [20, 22, 24, 31, 33, 35, 38, 64], aims to catch up with full fine-tuning by training a small number of parameters. Recently, this technique has emerged in the field of computer vision with promising results [7, 9, 12, 27–30, 36, 41, 71]. For example, VPT [27] adds learnable tokens, also called prompts, to the input sequence of one frozen transformer layer. Adapter [22] employs a bottleneck structure to adapt the pre-trained model. Some attempts also introduce parameterized hypercomplex multiplication layers [31] and re-parameterisation [44] to adapter-based methods. Moreover, LoRA [24] utilizes the low-rank nature of the incremental weight in attention and performs matrix decomposition for parameter efficiency. He *et al.* [20] go further to identify all the above three approaches from a unified perspective. In addition, NOAH [71] and GLoRA [7] introduce Neural Architecture Search (NAS) to combine different methods. SSF [36] performs a learnable affine transformation on features of the pre-trained model. FacT [29] tensorizes ViT and decomposes the increments into lightweight factors. Despite the great success of the above methods, it is worth noting that they have only proven to be effective in high-level visual understanding tasks. Therefore, performance degradation might occur when directly applying them to image restoration tasks due to the domain gap.

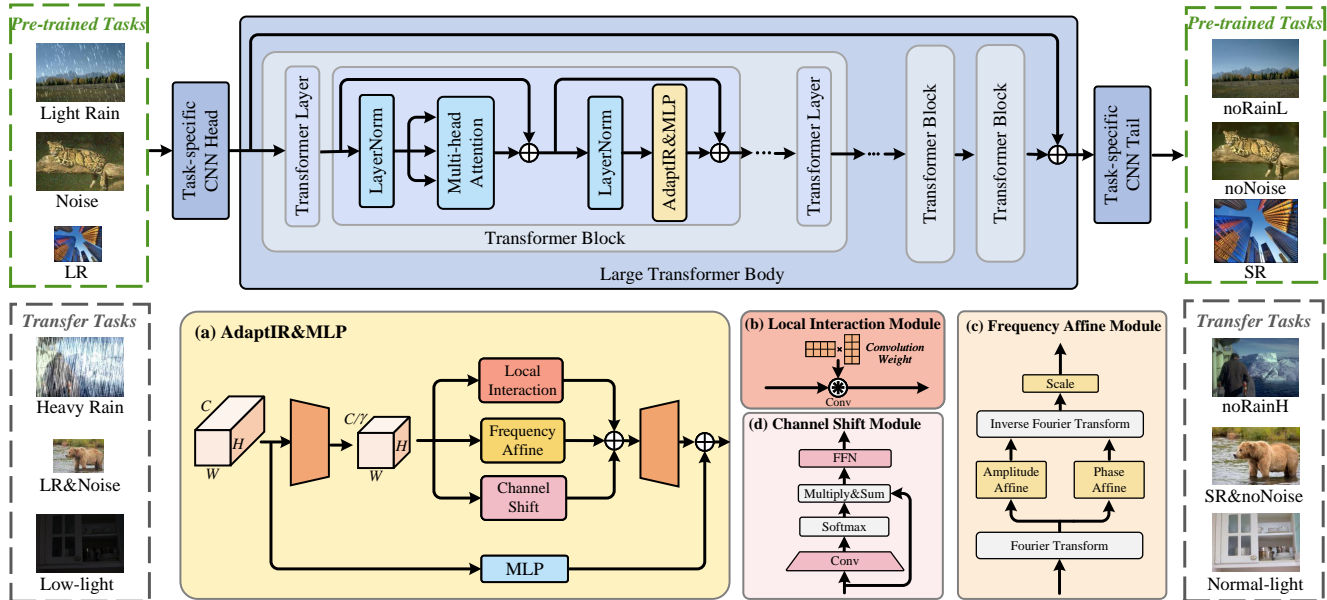


Figure 2. Overall pipeline. We include two task groups to cover various adaptation difficulties, namely i) Pre-trained Tasks, which have been seen during pre-training, and ii) Transfer Tasks, which have an unseen degradation level or type.

### 3. Method

#### 3.1. Preliminary

In this work, we aim to transfer the pre-trained image restoration model to downstream tasks using PETL techniques. As shown in Fig. 2, a typical pre-trained restoration model [8, 34] usually contains one large transformer body as well as task-specific CNN heads and tails. Given the pre-assigned task type, the low-quality image  $I_{LQ}$  will first go through the corresponding head to get the shallow feature  $X_{head}$ . After that,  $X_{head}$  is flattened into a 1D sequence on the spatial dimension and is input to the transformer body which contains several stacked transformer blocks with each block containing multiple transformer layers [58]. Finally, a skip connection is adopted followed by the task-specific tail to reconstruct the high-quality image  $I_{HQ}$ . During the pre-training stage, gradients from multiple tasks are used to update the shared body as well as the corresponding task-specific head and tail. After obtaining the pre-trained restoration model, in the fine-tuning stage of previous works, all parameters of the pre-trained model will be updated for specific downstream tasks, which burdens training and storage due to the per-task model weights.

#### 3.2. Adapting Pre-trained Restoration Models

We propose the AdaptIR, a plug-and-play module that is placed parallel to the frozen MLP in one transformer layer and can thus be seamlessly inserted into various ViT variants [19, 42]. More details will be given below.

**Orthogonal Inception Structure.** To formulate a PETL method applicable to diverse restoration tasks, we take inspiration from the Mixture-of-Experts (MoE) paradigm [32, 55, 72] and introduce a multi-branch inception structure, where each branch is an expert in dealing with degradation from a certain perspective and eventually achieve multi-pass property within one model (see Fig. 2(a)). Specifically, since the transformer body flattens the  $l$ -th layer feature into a 1D token sequence, we first restore the 2D image structure to obtain  $X_l \in \mathbb{R}^{C \times H \times W}$ . After that, we apply the  $1 \times 1$  convolution with channel reduction rate  $\gamma$  to transfer  $X_l$  to low-dimension intrinsic space and obtain the intrinsic feature  $X_l^{intrin} \in \mathbb{R}^{\frac{C}{\gamma} \times H \times W}$ . Then, three parallel branches are used to orthogonally model local spatial, global spatial, and channel interactions, which enables a powerful representation for hard tasks within a constrained parameter budget. At last, features from these three branches are ensembled to obtain  $X_l^{adapt}$  which will be added to the output of the frozen MLP to adapt the pre-trained restoration models.

**Local Interaction Module.** Image features usually possess neighborhood similarity, *i.e.*, the feature of one point tends to be similar to its surroundings. Therefore, a severely degraded feature point can refer to its neighborhood features to facilitate its restoration. Motivated by this observation, we introduce the Local Interaction Module (LIM) which uses the depth-separable  $3 \times 3$  convolution to model the local spatial prior (see Fig. 2(b)). Furthermore, we also experimentally find that the convolution kernel weights of LIM in AdaptIR exhibit a low-rank nature, and we thus utilize the low-rank decomposition to achieve parameter

reduction. Formally, given the convolution weight  $W \in \mathbb{R}^{C_{in} \times \frac{C_{out}}{group} \times K \times K}$ , where  $C_{in}$ ,  $C_{out}$  are input and output channel,  $K$  is the convolution kernel size and  $group$  is the number of convolution groups, we first reshape  $W$  into a 2D weight matrix  $W' \in \mathbb{R}^{C_{in} \times \frac{C_{out}}{group} K^2}$ , and then decompose  $W'$  into multiplication of two low-rank weight matrices:

$$W' = UV^T, \quad (1)$$

where  $U \in \mathbb{R}^{C_{in} \times r}$ ,  $V \in \mathbb{R}^{\frac{C_{out}}{group} K^2 \times r}$  and  $r$  is a predefined rank to trade-off performance and efficiency. Then we reshape  $W'$  to the original kernel size and use it to convolve  $X_l^{intrinsic}$  to get  $X_l^{ls}$ :

$$X_l^{ls} = \text{Reshape}(W') \otimes X_l^{intrinsic}, \quad (2)$$

where  $\otimes$  denotes convolution operator, and  $\text{Reshape}(\cdot)$  transforms 2D matrices into 4D convolution kernel weights.

**Frequency Affine Module.** Although the convolution operator can model spatial priors, it only employs local information. Intuitively, patch recurrence [48, 73] may happen between two distant patches. Therefore, modeling the global spatial prior can be beneficial for image restoration tasks [11, 37, 65]. A possible solution to this is to introduce the attention mechanism [58] which has a global receptive field. However, the attention comes at the cost of high complexity, which goes against the principle of parameter efficiency. In this work, we resort to the frequency domain for solution [13, 50, 53]. Specifically, we apply the Fast Fourier Transform (FFT) on  $X_l^{intrinsic}$  to obtain the corresponding frequency feature map  $X_l^F \in \mathbb{C}^{\frac{C}{\gamma} \times H \times (\lfloor \frac{W}{2} \rfloor + 1)}$ :

$$X_l^F(u, v) = \frac{1}{HW} \sum_{h=0}^{H-1} \sum_{w=0}^{W-1} X_l^{intrinsic}(h, w) e^{-2\pi i(\frac{uh}{H} + \frac{vw}{W})}, \quad (3)$$

As can be seen from Eq.3, a good property of FFT is that each position of the frequency feature map is the weighted sum of all features in the spatial domain. Therefore, performing pixel-wise projection on  $X_l^F$  is equivalent to performing a global operator in the spatial domain.

Motivated by this observation, we propose the Frequency Affine Module (FAM) to take advantage of the inherent global representation in  $X_l^F$  (see Fig. 2(c)). Concretely, we perform the affine transformation on amplitude map  $Mag_l$  and phase map  $Pha_l$  respectively with depth-separable  $1 \times 1$  convolution. To ensure numerical stability during the early training stages, we initialize the transformation layers as all-one weights and zero bias. Subsequently, the inverse Fast Fourier Transform (iFFT) is applied to convert the affined feature back to the spatial domain. Finally, another depth-separable  $1 \times 1$  convolution is used as a scale layer for subsequent feature ensemble. In short, the whole process can

be formalized as:

$$\begin{aligned} [Mag_l, Pha_l] &= \text{FFT}(X_l^{intrinsic}), \\ X_l^{gs} &= \text{Conv}(\text{iFFT}(\text{to\_complex}(\phi_1(Mag_l), \phi_2(Pha_l)))), \end{aligned} \quad (4)$$

where  $\phi_1(\cdot)$  and  $\phi_2(\cdot)$  are the frequency projection function and  $\text{to\_complex}(\cdot, \cdot)$  converts the magnitude and phase to complex numbers.

**Channel Shift Module.** The above LIM and FAM enable the pre-trained restoration models strong adaptation ability by exploiting local and global spatial priors. However, these two modules both adopt the depth-separable strategy for parameter efficiency, thus omitting the channel interaction. To allow for more powerful representation, we further develop the Channel Shift Module (CSM). As shown in Fig. 2(d), we first obtain the spatial weight mask  $\mathcal{M}_l \in \mathbb{R}^{1 \times H \times W}$  by employing  $1 \times 1$  convolution which compresses the channel dimension of  $X_l^{intrinsic}$  to 1, followed by the Softmax on the spatial dimension:

$$\mathcal{M}_l = \text{Softmax}(\text{Conv}(X_l^{intrinsic})), \quad (5)$$

We then utilize  $\mathcal{M}_l$  on each channel of  $X_l^{intrinsic}$  to perform spatially weighted summation to obtain the channel vector which will go through a Feed Forward Network (FFN) to generate the channel shifting factor  $X_l^c \in \mathbb{R}^{\frac{C}{\gamma} \times 1 \times 1}$ :

$$X_l^c = \text{FFN}\left(\sum_{h,w} \mathcal{M}_l \otimes X_l^{intrinsic}\right), \quad (6)$$

where  $\otimes$  denotes the Hadamard product.

**Feature Ensemble.** With the proposed multi-branch inception structure, the representations from three orthogonal branches can complement each other, and we further ensemble them in the intrinsic space with the summation to get the spatial-channel enriched ensemble feature  $X_l^{ensem}$ :

$$X_l^{ensem} = X_l^{ls} + X_l^{gs} + X_l^c \in \mathbb{R}^{\frac{C}{\gamma} \times H \times W}, \quad (7)$$

After that, a  $1 \times 1$  convolution is employed to up-dimension the  $X_l^{ensem}$  to generate adaptation feature  $X_l^{adapt} \in \mathbb{R}^{C \times H \times W}$ . Following [24, 70], we use zero to initialize the convolution weights. At last, the  $X_l^{adapt}$  is added to the output of the frozen MLP as residuals to adapt pre-trained restoration models to downstream tasks.

### 3.3. Parameter Efficient Training

During training, we freeze all parameters in the pre-trained model, including task-specific heads and tails as well as the transformer body except for the proposed AdaptIR.  $L_1$  loss is employed to provide pixel-level supervision:

$$L_{pix} = \|I_{HQ} - I_{LQ}\|_1, \quad (8)$$

where  $\|\cdot\|_1$  denotes  $L_1$  norm.

## 4. Experiment

In this section, we first evaluate on pre-trained tasks which contain image SR, color image denoising, and light rain streak removal. After that, we turn to more challenging transfer tasks, including heavy rain streak removal, second-order degradation, and low-light image enhancement. Furthermore, we conduct an ablation study to explore different parameter-efficient designs.

### 4.1. Experimental Settings

**Datasets.** For image SR, we choose DIV2K [1] and Flickr2K [57] as the training set, and we evaluate on Set5 [5], Set14 [66], BSDS100 [2], Urban100 [25], and Manga109 [47]. For color image denoising, training sets consist of DIV2K [1], Flickr2K [57], BSD400 [2], and WED [45], and we have two testing sets: CBSD68 [46] and Urban100 [25]. For image deraining, we evaluate using the Rain100L [62] and Rain100H [62] benchmarks, corresponding to light/heavy rain streaks. For second-order degradation, where one image contains two different degradation types, we choose low-resolution and noisy as representatives and synthesize degraded images by adding Gaussian noise to low-resolution images in the SR dataset. For low-light image enhancement, we utilize the training and testing set of LOLv1 [60]. More descriptions are given in the *supplementary material*.

**Evaluation Metrics.** We use the PSNR and SSIM to evaluate the effectiveness. The PSNR/SSIM of image SR, deraining, second-order degradation, and low-light image enhancement are computed on the Y channel from the YCbCr space, and we evaluate the RGB channel for denoising. Moreover, we use trainable #param to measure efficiency.

**Baseline Setup.** This work focuses on adapting pre-trained restoration models to downstream tasks under low parameter budgets. Since there is little work studying PETL on image restoration, we reproduce existing PETL approaches and compare them with the proposed AdaptIR. Specifically, we include the following representative PETL methods: **i)** VPT [27], where the learnable prompts are inserted as the input token of transformer layers, and we compare VPT<sub>Deep</sub> [27] in experiments because of its better performance. **ii)** Adapter [22], which introduces bottleneck structure placed after Attention and MLP. **iii)** LoRA [24], which adds parallel sub-networks to learn low-rank incremental matrices of query and value. **iv)** AdaptFormer [9], which inserts a tunable module parallel to MLP. **v)** SSF [36], where learnable scale and shift factors are used to modulate the frozen features. **vi)** FacT [29], which tensorises a ViT and then decomposes the incremental weights. In addition, we also present results of **vii)** full fine-tuning (Full-ft), and **viii)** directly applying pre-trained models to downstream tasks (Pretrain), to provide more insights.

Table 1. Quantitative comparison for *image super-resolution* on PSNR(dB). We compare the number of parameters when the performance is the same. **Best** and **second best** results are in red and blue colors, respectively.

Method	scale	#param	Set5	Set14	BSDS 100	Urban 100	Manga 109
Full-ft	×2	119M	38.39	34.56	32.54	33.98	39.90
Pretrain	×2	-	38.28	34.46	32.48	33.68	39.57
VPT [27]	×2	884K	38.35	34.47	32.48	34.74	39.77
Adapter [22]	×2	691K	38.36	34.50	32.48	33.73	39.80
LoRA [24]	×2	995K	38.38	34.52	32.49	33.76	39.80
AdaptFor. [9]	×2	677K	38.37	34.48	32.48	33.72	39.79
SSF [36]	×2	373K	37.47	33.06	31.82	30.85	37.46
FacT [29]	×2	537K	<b>38.38</b>	<b>34.52</b>	<b>32.49</b>	<b>33.76</b>	<b>39.83</b>
Ours	×2	370K	<b>38.38</b>	<b>34.51</b>	<b>32.49</b>	<b>33.77</b>	<b>39.82</b>
Full-ft	×3	119M	34.84	30.97	29.41	29.67	34.91
Pretrain	×3	-	34.66	30.80	29.32	29.39	34.38
VPT [27]	×3	884K	34.78	30.86	29.37	29.44	34.76
Adapter [22]	×3	691K	34.78	30.88	29.37	29.46	34.83
LoRA [24]	×3	995K	34.79	30.88	29.38	29.49	34.83
AdaptFor. [9]	×3	677K	34.78	30.88	29.37	29.45	34.81
SSF [36]	×3	373K	33.74	29.90	28.80	27.25	32.33
FacT [29]	×3	537K	<b>34.79</b>	<b>30.89</b>	<b>29.38</b>	<b>29.50</b>	<b>34.86</b>
Ours	×3	370K	<b>34.80</b>	<b>30.89</b>	<b>29.38</b>	<b>29.48</b>	<b>34.86</b>
Full-ft	×4	119M	32.66	29.03	27.82	27.31	31.64
Pretrain	×4	-	32.58	28.97	27.79	27.18	31.41
VPT [27]	×4	884K	32.70	29.02	27.82	27.20	31.65
Adapter [22]	×4	691K	32.70	29.03	27.82	27.21	31.68
LoRA [24]	×4	995K	32.70	29.03	27.82	27.22	31.68
AdaptFor. [9]	×4	677K	32.70	29.03	27.82	27.21	31.68
SSF [36]	×4	373K	31.57	28.20	27.30	25.38	29.36
FacT [29]	×4	537K	<b>32.71</b>	<b>29.03</b>	<b>27.82</b>	<b>27.23</b>	<b>31.70</b>
Ours	×4	370K	<b>32.71</b>	<b>29.04</b>	<b>27.82</b>	<b>27.22</b>	<b>31.70</b>

**Implementation Details.** We use two pre-trained restoration models, *i.e.*, IPT [8] and EDT [34], as the base models to evaluate different PETL methods. We control tunable parameters by adjusting channel reduction rate  $\gamma$ . We use AdamW [43] as the optimizer and train for 500 epochs. The learning rate is initialized to  $1e-4$  and decayed by half at {250,400,450,475} epochs.

### 4.2. Comparison on Pre-trained Tasks

We first compare the proposed AdaptIR with other PETL methods on pre-trained tasks that have been seen during pre-training. Following the setting in previous work [8, 34], we compare three restoration tasks, namely image SR, color image denoising, and light rain streak removal.

**Results on Super-resolution.** Tab. 1 shows the results. Our method outperforms the state-of-the-art method FacT [29] on most datasets and scales, while using the fewest parameters. Interestingly, in the  $\times 4$  setting, our method even attains better performance than full fine-tuning while using only 0.3% trainable parameters. Moreover, we also find that the performance of the recently proposed

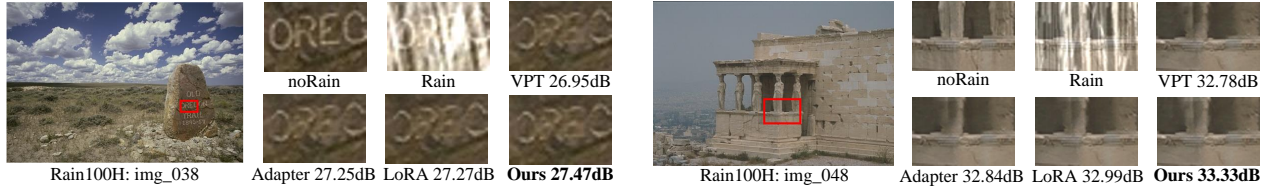


Figure 3. Visual comparison of *heavy rain streak removal* on samples from Rain100H [62] dataset.

Table 2. Quantitative comparison for *color image denoising* and *light rain streak removal* on PSNR(dB).

Method	#param	CBSD68		Urban100		Rain100L
		$\sigma=30$	$\sigma=50$	$\sigma=30$	$\sigma=50$	
Full-ft	119M	30.75	28.39	32.01	29.72	42.14
Pretrain	-	30.73	28.36	31.94	29.68	41.98
VPT [27]	884K	30.74	28.37	31.97	29.68	41.74
Adapter [22]	691K	30.74	28.37	31.97	29.69	41.95
LoRA [24]	995K	30.75	28.38	31.98	29.70	41.93
AdaptFor. [9]	677K	30.73	28.37	31.97	29.68	41.90
SSF [36]	373K	30.07	27.64	29.79	27.01	33.59
FacT [29]	537K	30.75	28.38	31.98	29.70	40.61
Ours	515K	30.74	28.38	31.98	29.69	41.99

SSF [36] is unsatisfactory. We argue that this is because SSF only uses transformation on channel dimension, without considering the spatial details that are important for restoration. This observation shows that directly taking current methods designed for visual understanding tasks to low-level restoration might yield sub-optimal results.

**Results on Denoising&DerainL.** We then evaluate the performance of color image denoising and light rain streak removal. Results are reported in Tab. 2. For denoising, our approach achieves comparable performance over different noise levels and datasets, while using fewer parameters. For light rain streak removal, our method outperforms the second best method [22] on the Rain100L [54] dataset. Surprisingly, the previously second best method FacT [29] suffers a severe performance degradation on this task, and a similar phenomenon can also be seen in the subsequent second-order degradation restoration and EDT as the base model. This observation suggests it is challenging for the existing methods to maintain consistent performance when changing downstream tasks or pre-trained models.

**Discussion on Pre-trained Tasks.** From the above experimental results on pre-trained tasks, it can be seen that the performance margin between different methods is not large. The main reason we argue is that the pre-trained model is already very powerful on these pre-trained tasks, so the improvement space left for evaluating the transfer ability of different PETL methods is very limited. For example, the pre-trained model is only 0.03 dB lower than full fine-tuning on  $\times 4$  SR with BSDS100 [2] dataset and even 0.02 dB on denoising with  $\sigma=30$  CBSD68 [46] dataset. The above observation leads to the following insights. i) The limited room for improvement leads to a small variance in

Table 3. Quantitative comparison for *heavy rain streak removal* on PSNR(dB).

Metric	Pretrain	VPT [27]	Adapter [22]	LoRA [24]	AdaptFor. [9]	FacT [29]	AdaptIR (ours)
#param	-	884K	691K	995K	677K	537K	933K
PSNR	17.30	30.87	30.99	31.16	31.10	29.70	31.28
SSIM	0.5488	0.8967	0.8971	0.9002	0.8992	0.8824	0.9022

the performance distribution, and thus even a slight absolute improvement on pre-trained tasks is statistically significant. ii) More challenging tasks, such as those not seen during the pre-training stage, are necessary to further evaluate the transfer capabilities of different PETL methods.

### 4.3. Comparison on Transfer Tasks

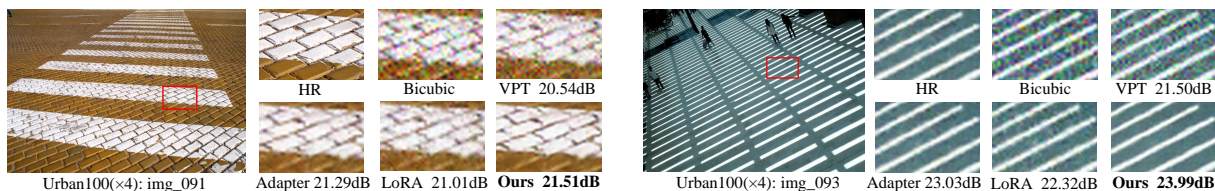
As discussed above, we further develop more challenging transfer tasks, which have an unseen degradation level or type, to evaluate different PETL approaches. Since few works are studying the transfer problem of pre-trained restoration models, we carefully design three transfer tasks with different difficulties.

**Unseen Degradation Levels.** We first design transfer tasks with the same degradation type as in pre-training but with an unseen level. Specifically, since the pre-trained model [8] is only trained on light rain streak removal, we therefore choose the deraining task with heavy rain streaks. As shown in Tab. 3, our AdaptIR surpasses the second best method LoRA [24] by 0.12dB with fewer parameters. Moreover, it can also be seen that the performance gap between different methods enlarges as the task becomes more difficult, which supports our previous analyses. We also give the quantitative comparison in Fig. 3.

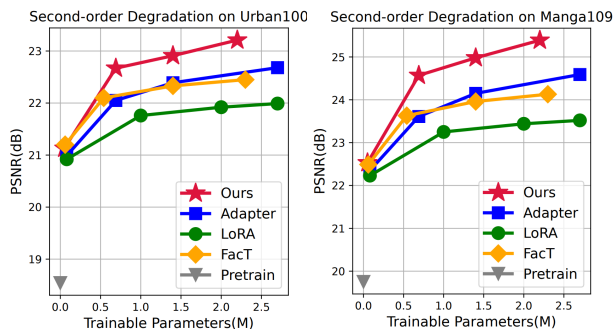
**Unseen Degradation Combinations.** In real-world scenarios, multiple degradations, or high-order degradation, are likely to occur in one single image [59]. Therefore, it is important to evaluate the performance of different PETL methods in this high-order degradation setting. In this work, we consider the second-order degradation for simplicity. Specifically, we combine two degradation types, *i.e.*,  $\times 4$  low-resolution and noise with  $\sigma=30$ , denoted as LR4&Noise30, to generate degraded images, where each degradation type is trained during pre-training, but their combination is unseen. The results, presented in Tab. 4, suggest that our approach achieves state-of-the-art performance with significant margins when the transfer task be-

Table 4. Quantitative comparison for *second-order degradation* with LR4&Noise30.

Method	Complexity		Set5		Set14		BSDS100		Urban100		Manga109	
	#param	FLOPs	PSNR	SSIM	PSNR	SSIM	PSNR	SSIM	PSNR	SSIM	PSNR	SSIM
Full-ft	119M	118.90G	27.24	0.7859	25.56	0.6686	25.02	0.6166	24.02	0.6967	26.31	0.8245
Pretrain	-	118.90G	19.74	0.3569	19.27	0.3114	19.09	0.2783	18.54	0.3254	19.75	0.3832
VPT [27]	884K	143.42G	24.11	0.5570	22.97	0.4722	22.91	0.4336	21.20	0.4527	22.61	0.5570
Adapter [22]	691K	119.92G	25.60	0.6862	24.16	0.5856	24.17	0.5498	22.05	0.5640	23.61	0.6904
LoRA [24]	995K	122.98G	25.19	0.6371	23.82	0.5405	23.82	0.5026	21.81	0.5193	23.30	0.6396
AdaptFormer [9]	677K	119.92G	<b>26.10</b>	<b>0.7138</b>	<b>24.58</b>	<b>0.6095</b>	<b>24.44</b>	<b>0.5686</b>	<b>22.52</b>	<b>0.5976</b>	<b>24.38</b>	<b>0.7296</b>
SSF [36]	373K	167.83G	25.41	0.6720	24.02	0.5761	24.06	0.5411	21.89	0.5514	23.33	0.6736
FacT [29]	537K	163.53G	25.70	0.6963	24.24	0.5944	24.25	0.5586	21.10	0.5727	23.63	0.6993
Ours	693K	119.93G	<b>26.46</b>	<b>0.7441</b>	<b>24.88</b>	<b>0.6345</b>	<b>24.67</b>	<b>0.5932</b>	<b>22.82</b>	<b>0.6279</b>	<b>24.80</b>	<b>0.7625</b>

Figure 4. Visual comparison of *second-order degradation* with LR4&Noise30 on samples from Urban100 [25] dataset.Table 5. Quantitative comparison for *low-light image enhancement* on PSNR(dB).

Metric	Pretrain	VPT [27]	Adapter [22]	LoRA [43]	AdaptFor. [9]	FacT [29]	AdaptIR (ours)
#param	-	884K	691K	995K	677K	537K	693K
PSNR	8.48	21.40	21.24	21.03	<b>21.53</b>	21.23	<b>21.56</b>
SSIM	0.2853	0.8098	0.8204	0.8097	<b>0.8225</b>	0.8187	<b>0.8415</b>

Figure 5. *Scalability comparison* with different PETL methods. We scale different methods by changing the dimension of hidden space for Adapter, FacT, and Ours, the number of tokens for VPT.

comes more difficult. For example, our method outperforms the second best method AdaptFormer [9] by 0.42 dB on Manga109 [47]. We also give several visual results in Fig. 4.

**Unseen Degradation Types.** We further assess different methods on degradation types that are unseen during pre-training, to further enlarge the domain gap. Specifically, we choose low-light image enhancement as the representative in this work. As shown in Tab. 5, our method continues to achieve the best results even with more challenging unseen

Table 6. Comparison on generalisation ability with *more pre-trained base models*. EDT is used as the base model and evaluated on second-order degradation with LR4&Noise30 on PSNR(dB).

Method	#param	Set5	Set14	BSDS 100	Urban 100	Manga 109
Full-ft	11.6M	27.32	25.60	25.03	24.10	26.42
Pretrain	-	19.29	18.45	18.27	17.92	19.25
VPT [27]	311K	24.19	22.91	22.81	21.12	22.49
Adapter [22]	194K	26.92	25.27	24.81	23.48	25.84
LoRA [24]	259K	26.91	25.25	24.80	23.46	25.81
AdaptFor. [9]	162K	<b>26.99</b>	<b>25.31</b>	<b>24.85</b>	<b>23.59</b>	<b>25.95</b>
SSF [36]	117K	26.92	25.24	24.83	23.41	25.77
FacT [29]	174K	26.89	25.25	24.81	23.43	25.78
Ours	170K	<b>27.04</b>	<b>25.36</b>	<b>24.88</b>	<b>23.63</b>	<b>26.00</b>

degradation types. In addition, compared to the unsatisfactory result of 8.48dB for zero-shot transfer of the pre-trained model, the proposed method achieves a performance improvement of 13.08dB with only training 0.6% parameters, demonstrating the potential of PETL in image restoration. We also give some visual results in Fig. 6.

#### 4.4. Generalization Ability

**Scaling Trainable Parameters.** We compare the performance of different methods under varying parameter budgets. We use the second-order degradation, *i.e.* LR4&Noise30, in this setup. Fig. 5 shows the results. It can be seen that the proposed method surpasses other strong baselines across various parameter settings, demonstrating the strong scalability of the proposed method.

**Results on More Pre-trained Models.** The above experiments employ IPT [8] as the base model. In order to verify

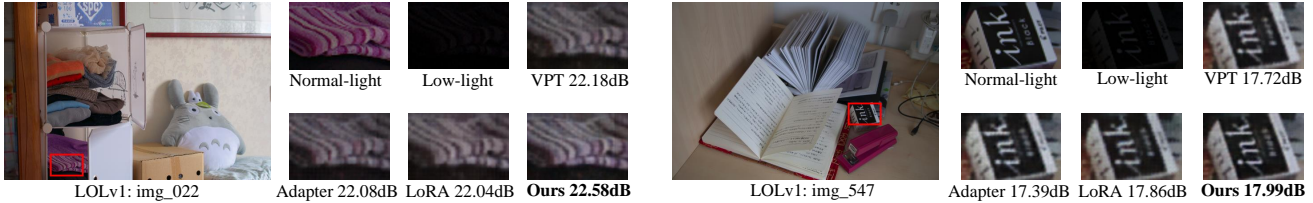


Figure 6. Visual comparison of low-light image enhancement on samples from LOLv1 [60] dataset.

Table 7. Ablation experiments for the proposed parameter efficient designs on PSNR(dB). *Baseline* refers to the setting of depth-separable projection in LIM and FAM, as well as low-rank decomposition and channel-spatial orthogonal modeling.

Settings	#param	Set5	Set14	Urban100
(0)Baseline	686K	26.23	24.67	22.56
(1)+w/o decomposition in LIM	689K	26.01	24.47	22.32
(2)+w/o depth-separable in LIM	718K	25.67	24.22	22.10
(3)+w/o depth-separable in FAM	728K	25.73	24.28	22.17
(4)+w/o CSM&w/o depth-separable	743K	24.26	23.15	21.36

the generalization of the proposed method, we further adopt another pre-trained image restoration model EDT [34] as the frozen base model. Tab. 6 represents the results. It can be seen that the proposed method maintains state-of-the-art performance by tuning only 1.5% parameters when replaced with another pre-trained model. More experiments with EDT can be seen in the *supplementary material*.

#### 4.5. Ablation Study

We ablate our method to identify the effect of different designs. The ablation experiments are conducted on the second-order degradation with LR4&Noise30 using IPT [8] as the pre-trained base model.

**Parameter Efficient Designs.** In this work, we introduce several techniques to achieve parameter efficiency, such as low-rank decomposition on convolution weights, depth-separable strategy, and spatial-channel orthogonal modeling. We ablate to study the parameter-performance trade-off of these choices. The results, presented in Tab. 7, indicate that (1) using full convolution kernel weights in LIM even leads to a performance drop, demonstrating the weight redundancy of the convolution kernel in AdaptIR. In addition, (2)&(3) removing the depth-separable design in LIM or FAM will conflict with the channel modeling in CSM, and lead to sub-optimal results. Further, (4) removing the CSM branch while allowing full-channel interaction in other branches results in poor performance, which we attribute to the learning difficulty of modeling channel and spatial simultaneously.

**Ablation for Components.** In the proposed AdaptIR, three parallel branches are developed, where each branch functions as an expert and respectively models local spatial, global spatial and channel interactions in an orthogonal manner. We ablate to discern the roles of different

Table 8. Ablation experiments for the effectiveness of different components on PSNR(dB).

LIM	FAM	CSM	#param	Set5	Set14	Urban100
		✓	680K	23.64	22.66	20.97
	✓	✓	682K	25.52	24.17	22.05
✓	✓		678K	26.11	24.60	22.52
✓	✓	✓	692K	26.46	24.88	22.82

Table 9. Ablation experiments for different insertion positions and forms on PSNR(dB).

position	form	Set5	Set14	Urban100
MLP	parallel	26.45	24.88	22.82
Attention	parallel	26.28	24.70	22.59
MLP	sequential	26.35	24.77	22.67
Attention	sequential	25.60	24.19	22.07

branches. As shown in Tab. 8, separate utilization of one or two branches only yields sub-optimal results owing to the insufficient representation. And the combination of the three branches achieves the best results.

**Insertion Position and Form.** In the current adapter-based approaches [9, 22, 56], various options exist for both the insertion location and form of adapters. The impact of these choices is shown in Tab. 9. It can be seen that inserting an adapter into MLP achieves better performance under both parallel and sequential forms. This is because there is a certain dependency between the well-trained MLP and attention, and insertion into the middle of them will damage this relationship. Moreover, the parallel insertion form performs better than its sequential counterpart. We argue that parallel form can preserve the knowledge of frozen features through summation, thus reducing the learning difficulty.

## 5. Conclusion

In this work, we explore for the first time the parameter-efficient adaptation of pre-trained image restoration models on various downstream tasks, to address the costly training and storage challenges posed by full fine-tuning. In order to achieve multi-degradation universality and powerful representation, a novel multi-branch inception structure is proposed to orthogonally model the local spatial, global spatial, and channel dependencies. Extensive experiments validate our AdaptIR as a versatile and powerful adaptation solution.



## References

- [1] Eirikur Agustsson and Radu Timofte. Ntire 2017 challenge on single image super-resolution: Dataset and study. In *Proceedings of the IEEE conference on computer vision and pattern recognition workshops*, pages 126–135, 2017. [5](#)
- [2] Pablo Arbelaez, Michael Maire, Charless Fowlkes, and Jitendra Malik. Contour detection and hierarchical image segmentation. *IEEE transactions on pattern analysis and machine intelligence*, 33(5):898–916, 2010. [5](#), [6](#)
- [3] Akari Asai, Mohammadreza Salehi, Matthew E Peters, and Hannaneh Hajishirzi. Attempt: Parameter-efficient multi-task tuning via attentional mixtures of soft prompts. In *Proceedings of the 2022 Conference on Empirical Methods in Natural Language Processing*, pages 6655–6672, 2022. [1](#)
- [4] Hangbo Bao, Li Dong, Songhao Piao, and Furu Wei. Beit: Bert pre-training of image transformers. *arXiv preprint arXiv:2106.08254*, 2021. [2](#)
- [5] Marco Bevilacqua, Aline Roumy, Christine Guillemot, and Marie Line Alberi-Morel. Low-complexity single-image super-resolution based on nonnegative neighbor embedding. 2012. [5](#)
- [6] Tom Brown, Benjamin Mann, Nick Ryder, Melanie Subbiah, Jared D Kaplan, Prafulla Dhariwal, Arvind Neelakantan, Pranav Shyam, Girish Sastry, Amanda Askell, et al. Language models are few-shot learners. *Advances in neural information processing systems*, 33:1877–1901, 2020. [2](#)
- [7] Arnav Chavan, Zhuang Liu, Deepak Gupta, Eric Xing, and Zhiqiang Shen. One-for-all: Generalized lora for parameter-efficient fine-tuning. *arXiv preprint arXiv:2306.07967*, 2023. [2](#)
- [8] Hanting Chen, Yunhe Wang, Tianyu Guo, Chang Xu, Yiping Deng, Zhenhua Liu, Siwei Ma, Chunjing Xu, Chao Xu, and Wen Gao. Pre-trained image processing transformer. In *Proceedings of the IEEE/CVF conference on computer vision and pattern recognition*, pages 12299–12310, 2021. [1](#), [2](#), [3](#), [5](#), [6](#), [7](#), [8](#)
- [9] Shoufa Chen, Chongjian Ge, Zhan Tong, Jiangliu Wang, Yibing Song, Jue Wang, and Ping Luo. Adaptorformer: Adapting vision transformers for scalable visual recognition. *Advances in Neural Information Processing Systems*, 35:16664–16678, 2022. [2](#), [5](#), [6](#), [7](#), [8](#)
- [10] Wentao Chen, Chenyang Si, Zhang Zhang, Liang Wang, Zilei Wang, and Tieniu Tan. Semantic prompt for few-shot image recognition. In *Proceedings of the IEEE/CVF Conference on Computer Vision and Pattern Recognition*, pages 23581–23591, 2023. [1](#)
- [11] Xiangyu Chen, Xintao Wang, Jiantao Zhou, and Chao Dong. Activating more pixels in image super-resolution transformer. *arxiv* 2022. *arXiv preprint arXiv:2205.04437*, 1, 2022. [4](#)
- [12] Zhe Chen, Yuchen Duan, Wenhai Wang, Junjun He, Tong Lu, Jifeng Dai, and Yu Qiao. Vision transformer adapter for dense predictions. *arXiv preprint arXiv:2205.08534*, 2022. [1](#), [2](#)
- [13] Lu Chi, Borui Jiang, and Yadong Mu. Fast fourier convolution. *Advances in Neural Information Processing Systems*, 33:4479–4488, 2020. [4](#)
- [14] Tao Dai, Jianrui Cai, Yongbing Zhang, Shu-Tao Xia, and Lei Zhang. Second-order attention network for single image super-resolution. In *Proceedings of the IEEE/CVF conference on computer vision and pattern recognition*, pages 11065–11074, 2019. [2](#)
- [15] Jia Deng, Wei Dong, Richard Socher, Li-Jia Li, Kai Li, and Li Fei-Fei. Imagenet: A large-scale hierarchical image database. In *2009 IEEE conference on computer vision and pattern recognition*, pages 248–255. Ieee, 2009. [1](#), [2](#)
- [16] Zeshuai Deng, Zhuokun Chen, Shuaicheng Niu, Thomas H Li, Bohan Zhuang, and Mingkui Tan. Efficient test-time adaptation for super-resolution with second-order degradation and reconstruction. In *Thirty-seventh Conference on Neural Information Processing Systems*, 2023. [2](#)
- [17] Jacob Devlin, Ming-Wei Chang, Kenton Lee, and Kristina Toutanova. Bert: Pre-training of deep bidirectional transformers for language understanding. *arXiv preprint arXiv:1810.04805*, 2018. [2](#)
- [18] Chao Dong, Chen Change Loy, Kaiming He, and Xiaoou Tang. Learning a deep convolutional network for image super-resolution. In *Computer Vision—ECCV 2014: 13th European Conference, Zurich, Switzerland, September 6–12, 2014, Proceedings, Part IV 13*, pages 184–199. Springer, 2014. [1](#)
- [19] Alexey Dosovitskiy, Lucas Beyer, Alexander Kolesnikov, Dirk Weissenborn, Xiaohua Zhai, Thomas Unterthiner, Mostafa Dehghani, Matthias Minderer, Georg Heigold, Sylvain Gelly, et al. An image is worth 16x16 words: Transformers for image recognition at scale. *arXiv preprint arXiv:2010.11929*, 2020. [3](#)
- [20] Junxian He, Chunting Zhou, Xuezhe Ma, Taylor Berg-Kirkpatrick, and Graham Neubig. Towards a unified view of parameter-efficient transfer learning. *arXiv preprint arXiv:2110.04366*, 2021. [2](#)
- [21] Kaiming He, Xinlei Chen, Saining Xie, Yanghao Li, Piotr Dollár, and Ross Girshick. Masked autoencoders are scalable vision learners. In *Proceedings of the IEEE/CVF conference on computer vision and pattern recognition*, pages 16000–16009, 2022. [2](#)
- [22] Neil Houlsby, Andrei Giurgiu, Stanislaw Jastrzebski, Bruna Morrone, Quentin De Laroussilhe, Andrea Gesmundo, Mona Attariyan, and Sylvain Gelly. Parameter-efficient transfer learning for nlp. In *International Conference on Machine Learning*, pages 2790–2799. PMLR, 2019. [1](#), [2](#), [5](#), [6](#), [7](#), [8](#)
- [23] Andrew G Howard, Menglong Zhu, Bo Chen, Dmitry Kalenichenko, Weijun Wang, Tobias Weyand, Marco Andreetto, and Hartwig Adam. Mobilenets: Efficient convolutional neural networks for mobile vision applications. *arXiv preprint arXiv:1704.04861*, 2017. [2](#)
- [24] Edward J Hu, Yelong Shen, Phillip Wallis, Zeyuan Allen-Zhu, Yuanzhi Li, Shean Wang, Lu Wang, and Weizhu Chen. Lora: Low-rank adaptation of large language models. *arXiv preprint arXiv:2106.09685*, 2021. [2](#), [4](#), [5](#), [6](#), [7](#)
- [25] Jia-Bin Huang, Abhishek Singh, and Narendra Ahuja. Single image super-resolution from transformed self-exemplars. In *Proceedings of the IEEE conference on computer vision and pattern recognition*, pages 5197–5206, 2015. [5](#), [7](#)

- [26] Siteng Huang, Biao Gong, Yulin Pan, Jianwen Jiang, Yiliang Lv, Yuyuan Li, and Donglin Wang. Vop: Text-video co-operative prompt tuning for cross-modal retrieval. In *Proceedings of the IEEE/CVF Conference on Computer Vision and Pattern Recognition*, pages 6565–6574, 2023. [2](#)
- [27] Menglin Jia, Luming Tang, Bor-Chun Chen, Claire Cardie, Serge Belongie, Bharath Hariharan, and Ser-Nam Lim. Visual prompt tuning. In *European Conference on Computer Vision*, pages 709–727. Springer, 2022. [2](#), [5](#), [6](#), [7](#)
- [28] Shibo Jie and Zhi-Hong Deng. Convolutional bypasses are better vision transformer adapters. *arXiv preprint arXiv:2207.07039*, 2022.
- [29] Shibo Jie and Zhi-Hong Deng. Fact: Factor-tuning for lightweight adaptation on vision transformer. In *Proceedings of the AAAI Conference on Artificial Intelligence*, pages 1060–1068, 2023. [2](#), [5](#), [6](#), [7](#)
- [30] Shibo Jie, Haoqing Wang, and Zhi-Hong Deng. Revisiting the parameter efficiency of adapters from the perspective of precision redundancy. In *Proceedings of the IEEE/CVF International Conference on Computer Vision*, pages 17217–17226, 2023. [2](#)
- [31] Rabeeh Karimi Mahabadi, James Henderson, and Sebastian Ruder. Compacter: Efficient low-rank hypercomplex adapter layers. *Advances in Neural Information Processing Systems*, 34:1022–1035, 2021. [1](#), [2](#)
- [32] Sneha Kudugunta, Yanping Huang, Ankur Bapna, Maxim Krikun, Dmitry Lepikhin, Minh-Thang Luong, and Orhan Firat. Beyond distillation: Task-level mixture-of-experts for efficient inference. *arXiv preprint arXiv:2110.03742*, 2021. [2](#), [3](#)
- [33] Brian Lester, Rami Al-Rfou, and Noah Constant. The power of scale for parameter-efficient prompt tuning. *arXiv preprint arXiv:2104.08691*, 2021. [2](#)
- [34] Wenbo Li, Xin Lu, Shengju Qian, Jiangbo Lu, Xiangyu Zhang, and Jiaya Jia. On efficient transformer-based image pre-training for low-level vision. *arXiv preprint arXiv:2112.10175*, 2021. [1](#), [2](#), [3](#), [5](#), [8](#)
- [35] Xiang Lisa Li and Percy Liang. Prefix-tuning: Optimizing continuous prompts for generation. *arXiv preprint arXiv:2101.00190*, 2021. [2](#)
- [36] Dongze Lian, Daquan Zhou, Jiashi Feng, and Xinchao Wang. Scaling & shifting your features: A new baseline for efficient model tuning. *Advances in Neural Information Processing Systems*, 35:109–123, 2022. [2](#), [5](#), [6](#), [7](#)
- [37] Jingyun Liang, Jiezhong Cao, Guolei Sun, Kai Zhang, Luc Van Gool, and Radu Timofte. Swinir: Image restoration using swin transformer. In *Proceedings of the IEEE/CVF international conference on computer vision*, pages 1833–1844, 2021. [4](#)
- [38] Pengfei Liu, Weizhe Yuan, Jinlan Fu, Zhengbao Jiang, Hiroaki Hayashi, and Graham Neubig. Pre-train, prompt, and predict: A systematic survey of prompting methods in natural language processing. *ACM Computing Surveys*, 55(9): 1–35, 2023. [2](#)
- [39] Yihao Liu, Xiangyu Chen, Xianzheng Ma, Xintao Wang, Jiantao Zhou, Yu Qiao, and Chao Dong. Unifying image processing as visual prompting question answering. *arXiv preprint arXiv:2310.10513*, 2023. [2](#)
- [40] Yihao Liu, Jingwen He, Jinjin Gu, Xiangtao Kong, Yu Qiao, and Chao Dong. Degae: A new pretraining paradigm for low-level vision. In *Proceedings of the IEEE/CVF Conference on Computer Vision and Pattern Recognition*, pages 23292–23303, 2023. [2](#)
- [41] Yen-Cheng Liu, Chih-Yao Ma, Junjiao Tian, Zijian He, and Zsolt Kira. Polyhistor: Parameter-efficient multi-task adaptation for dense vision tasks. *Advances in Neural Information Processing Systems*, 35:36889–36901, 2022. [1](#), [2](#)
- [42] Ze Liu, Yutong Lin, Yue Cao, Han Hu, Yixuan Wei, Zheng Zhang, Stephen Lin, and Baining Guo. Swin transformer: Hierarchical vision transformer using shifted windows. In *Proceedings of the IEEE/CVF international conference on computer vision*, pages 10012–10022, 2021. [3](#)
- [43] Ilya Loshchilov and Frank Hutter. Decoupled weight decay regularization. *arXiv preprint arXiv:1711.05101*, 2017. [5](#), [7](#)
- [44] Gen Luo, Minglang Huang, Yiyi Zhou, Xiaoshuai Sun, Guannan Jiang, Zhiyu Wang, and Rongrong Ji. Towards efficient visual adaptation via structural re-parameterization. *arXiv preprint arXiv:2302.08106*, 2023. [2](#)
- [45] Kede Ma, Zhengfang Duanmu, Qingbo Wu, Zhou Wang, Hongwei Yong, Hongliang Li, and Lei Zhang. Waterloo exploration database: New challenges for image quality assessment models. *IEEE Transactions on Image Processing*, 26(2):1004–1016, 2016. [5](#)
- [46] David Martin, Charless Fowlkes, Doron Tal, and Jitendra Malik. A database of human segmented natural images and its application to evaluating segmentation algorithms and measuring ecological statistics. In *Proceedings Eighth IEEE International Conference on Computer Vision. ICCV 2001*, pages 416–423. IEEE, 2001. [5](#), [6](#)
- [47] Yusuke Matsui, Kota Ito, Yuji Aramaki, Azuma Fujimoto, Toru Ogawa, Toshihiko Yamasaki, and Kiyoharu Aizawa. Sketch-based manga retrieval using manga109 dataset. *Multimedia Tools and Applications*, 76:21811–21838, 2017. [5](#), [7](#)
- [48] Tomer Michaeli and Michal Irani. Nonparametric blind super-resolution. In *Proceedings of the IEEE International Conference on Computer Vision*, pages 945–952, 2013. [2](#), [4](#)
- [49] Dongwon Park, Byung Hyun Lee, and Se Young Chun. All-in-one image restoration for unknown degradations using adaptive discriminative filters for specific degradations. In *2023 IEEE/CVF Conference on Computer Vision and Pattern Recognition (CVPR)*, pages 5815–5824. IEEE, 2023. [2](#)
- [50] Namuk Park and Songkuk Kim. How do vision transformers work? In *International Conference on Learning Representations*, 2021. [4](#)
- [51] Alec Radford, Karthik Narasimhan, Tim Salimans, Ilya Sutskever, et al. Improving language understanding by generative pre-training. 2018. [2](#)
- [52] Alec Radford, Jeffrey Wu, Rewon Child, David Luan, Dario Amodei, Ilya Sutskever, et al. Language models are unsupervised multitask learners. *OpenAI blog*, 1(8):9, 2019. [2](#)
- [53] Yongming Rao, Wenliang Zhao, Zheng Zhu, Jiwen Lu, and Jie Zhou. Global filter networks for image classification. *Advances in neural information processing systems*, 34:980–993, 2021. [4](#)

- [54] Dongwei Ren, Wangmeng Zuo, Qinghua Hu, Pengfei Zhu, and Deyu Meng. Progressive image deraining networks: A better and simpler baseline. In *Proceedings of the IEEE/CVF conference on computer vision and pattern recognition*, pages 3937–3946, 2019. 1, 6
- [55] Carlos Riquelme, Joan Puigcerver, Basil Mustafa, Maxim Neumann, Rodolphe Jenatton, André Susano Pinto, Daniel Keysers, and Neil Houlsby. Scaling vision with sparse mixture of experts. *Advances in Neural Information Processing Systems*, 34:8583–8595, 2021. 2, 3
- [56] Asa Cooper Stickland and Iain Murray. Bert and pals: Projected attention layers for efficient adaptation in multi-task learning. In *International Conference on Machine Learning*, pages 5986–5995. PMLR, 2019. 8
- [57] Radu Timofte, Eirikur Agustsson, Luc Van Gool, Ming-Hsuan Yang, and Lei Zhang. Ntire 2017 challenge on single image super-resolution: Methods and results. In *Proceedings of the IEEE conference on computer vision and pattern recognition workshops*, pages 114–125, 2017. 5
- [58] Ashish Vaswani, Noam Shazeer, Niki Parmar, Jakob Uszkoreit, Llion Jones, Aidan N Gomez, Łukasz Kaiser, and Illia Polosukhin. Attention is all you need. *Advances in neural information processing systems*, 30, 2017. 3, 4
- [59] Xintao Wang, Liangbin Xie, Chao Dong, and Ying Shan. Real-esrgan: Training real-world blind super-resolution with pure synthetic data. In *Proceedings of the IEEE/CVF international conference on computer vision*, pages 1905–1914, 2021. 2, 6
- [60] Chen Wei, Wenjing Wang, Wenhan Yang, and Jiaying Liu. Deep retinex decomposition for low-light enhancement. *arXiv preprint arXiv:1808.04560*, 2018. 5, 8
- [61] Zhenda Xie, Zheng Zhang, Yue Cao, Yutong Lin, Jianmin Bao, Zhuliang Yao, Qi Dai, and Han Hu. Simmim: A simple framework for masked image modeling. In *Proceedings of the IEEE/CVF Conference on Computer Vision and Pattern Recognition*, pages 9653–9663, 2022. 2
- [62] Wenhan Yang, Robby T Tan, Jiashi Feng, Zongming Guo, Shuicheng Yan, and Jiaying Liu. Joint rain detection and removal from a single image with contextualized deep networks. *IEEE transactions on pattern analysis and machine intelligence*, 42(6):1377–1393, 2019. 2, 5, 6
- [63] Hanrong Ye and Dan Xu. Taskprompter: Spatial-channel multi-task prompting for dense scene understanding. In *The Eleventh International Conference on Learning Representations*, 2022. 2
- [64] Elad Ben Zaken, Shauli Ravfogel, and Yoav Goldberg. Bitfit: Simple parameter-efficient fine-tuning for transformer-based masked language-models. *arXiv preprint arXiv:2106.10199*, 2021. 2
- [65] Syed Waqas Zamir, Aditya Arora, Salman Khan, Munawar Hayat, Fahad Shahbaz Khan, and Ming-Hsuan Yang. Restormer: Efficient transformer for high-resolution image restoration. In *Proceedings of the IEEE/CVF conference on computer vision and pattern recognition*, pages 5728–5739, 2022. 4
- [66] Roman Zeyde, Michael Elad, and Matan Protter. On single image scale-up using sparse-representations. In *Curves and Surfaces: 7th International Conference, Avignon, France, June 24-30, 2010, Revised Selected Papers 7*, pages 711–730. Springer, 2012. 5
- [67] Yaohua Zha, Jinpeng Wang, Tao Dai, Bin Chen, Zhi Wang, and Shu-Tao Xia. Instance-aware dynamic prompt tuning for pre-trained point cloud models. *arXiv preprint arXiv:2304.07221*, 2023. 1
- [68] Kai Zhang, Wangmeng Zuo, Yunjin Chen, Deyu Meng, and Lei Zhang. Beyond a gaussian denoiser: Residual learning of deep cnn for image denoising. *IEEE transactions on image processing*, 26(7):3142–3155, 2017. 1, 2
- [69] Kai Zhang, Wangmeng Zuo, Shuhang Gu, and Lei Zhang. Learning deep cnn denoiser prior for image restoration. In *Proceedings of the IEEE conference on computer vision and pattern recognition*, pages 3929–3938, 2017. 2
- [70] Lvmin Zhang, Anyi Rao, and Maneesh Agrawala. Adding conditional control to text-to-image diffusion models. In *Proceedings of the IEEE/CVF International Conference on Computer Vision*, pages 3836–3847, 2023. 4
- [71] Yuanhan Zhang, Kaiyang Zhou, and Ziwei Liu. Neural prompt search. 2022. 2
- [72] Jinguo Zhu, Xizhou Zhu, Wenhai Wang, Xiaohua Wang, Hongsheng Li, Xiaogang Wang, and Jifeng Dai. Uni-perceiver-moe: Learning sparse generalist models with conditional moes. *Advances in Neural Information Processing Systems*, 35:2664–2678, 2022. 2, 3
- [73] Maria Zontak and Michal Irani. Internal statistics of a single natural image. In *CVPR 2011*, pages 977–984. IEEE, 2011. 2, 4